Turkish Journal of Electrical Engineering and Computer Sciences

Volume 31 | Number 7 Article 7

11-30-2023

A novel computing scheme based on pattern matching for identification of nephron loss and chronic kidney disease stage

REHAN AHMAD

BASANT MOHANTY

Turkish Journal of Electrical Engineering & Computer Sciences

http://journals.tubitak.gov.tr/elektrik/

Research Article

Turk J Elec Eng & Comp Sci
(2023) 31: 1237 – 1254

doi:10.55730/1300-0632.4045

A novel computing scheme based on pattern matching for identification of nephron loss and chronic kidney disease stage

Rehan AHMAD[1,*], **Basant K. MOHANTY**[2]
[1]Mukesh Patel School of Technology Management and Engineering,
Shri Vile Parle Kelavani Mandal's Narsee Monjee Institute of Management Studies, Shirpur, India
[2]Sambalpur University Institute of Information Technology, Burla, Sambalpur, Orissa, India

Received: 24.02.2023 • **Accepted/Published Online:** 26.09.2023 • **Final Version:** 30.11.2023

Abstract: Nephrons are the basic filtering units of the kidneys. Progression of chronic kidney disease (CKD) destroys nephrons permanently. Although there are many computing schemes suggested in recent years to identify CKD stages, no computing method has been suggested for identifying the nephron loss within kidney regions during CKD progression. In this paper, a novel pattern matching-based computation scheme is proposed to detect nephron loss in the kidney regions during CKD progression. We consider image registration (IR) with different transforms and a structural similarity index algorithm (SSIM) to match patterns of ultrasound images of kidney regions to identify the nephron loss. Simulation results show that the proposed scheme based on IR and SSIM algorithms detects almost 34% and 51% and almost 35% and 56% of the nephron damage in the cortex and medulla relative to a normal kidney, respectively. We extend the pattern matching scheme to identify CKD stages, as well. The proposed scheme based on IR and the SSIM algorithm can identify CKD stage with accuracy of 96% and 88%, respectively. The prediction accuracy of the proposed scheme for identifying CKD stage is comparable to that of the gray level co-occurrence matrix-based method, which is the best among the existing computing methods. However, the proposed scheme has advantages over the preexisting scheme, such as: the proposed method can be used to identify both CKD stage and the nephron loss in different kidney regions, and it identifies CKD stage without using a classifier. Therefore, the proposed pattern matching-based computing method is a better alternative to existing computing schemes for CKD stage identification.

Key words: Nephron, chronic kidney disease, ultrasound image, image registration, structural similarity index

1. Introduction

Nephrons are basic building elements of the human kidney. Nephrons filter out toxic elements from the impure blood and retain nutrients required for the body. A healthy human kidney has about 2 million nephrons, but there is wide variability according to race, region, and ethnicity [1]. The average nephron number could vary in the approximate range of 2 million to 2.5 million [2]. The cortex and medulla are the two important regions of the human kidney. Two types of nephrons exist according to their presence at specific locations in the human kidney: cortical nephrons (found in the cortex) and juxtamedullary nephrons (found in the medulla) [3]. The pelvis is also an integral region of the kidney, and it is made up of pelvis cells, not nephrons [3]. Chronic kidney disease (CKD) is a silent disease that destroys the functioning capability of nephrons [3]. CKD is categorized into five stages (stage-1, stage-2, stage-3, stage-4, and stage-5). Stage-1 indicates the primary stage of CKD

*Correspondence: rehan.ahmad@nmims.edu

and stage-2 indicates progression of the kidneys towards a critical state. Stage-3 indicates the beginning of the critical stage while stage-4 indicates that the kidneys are in a critical state. Stage-5 indicates kidney dysfunction leading to kidney failure [3]. Early detection of nephron loss could help nephrologists visualize the amount of damage in the kidney regions and advise the patient accordingly to start treatment [4]. The impact of CKD progression is viewed as nephron loss. Nephron loss can be identified through the glomerular filtration rate (GFR) method and biopsy [5]. The GFR method uses blood and urine samples of the patient. In this method, the amount of toxicity present in the blood and the amount of urine produced by the kidneys are estimated for CKD stage identification. GFR values are in the unit mL/min/1.73 m^2. GFR values in the range of 100–120 represent healthy kidneys, while GFR values in the ranges of 90–99, 60–89, 30–59, 15–29, and below 15 represent CKD stage-1, stage-2, stage-3, stage-4, and stage-5, respectively. In the biopsy method, sample kidney tissues are extracted from the region under examination [5]. These two methods are invasive, expensive, and time-consuming and they require a certain controlled environment to produce accurate results. Patients suffering from CKD and associated ailments are sometimes not in a proper mental state for these tests. An alternative imaging approach to estimate nephron loss to access the impact of CKD on internal kidney regions (the cortex and medulla) is required, which could be less expensive, less time-consuming, and independent of human expertise. Ultrasound (US) imaging is a noninvasive, radiation-free, infection-free, and less costly method compared to biopsy and GFR clinical processes [4]. Through US imaging, kidney tissue damage can be observed directly. Some patients' blood examinations might yield normal results but their kidney tissues are nevertheless damaged. This damage will result in the quick progression of CKD stages and cannot be observed from blood examinations [6]. US images are able to capture significant amounts of information about internal kidney regions such as the cortex and medulla in terms of gray-scale intensity distribution. US kidney images also provide relevant information related to the impact of CKD stage progression on kidney internal regions [6]. In recent years, computational methods have been suggested to identify different kidney diseases, including CKD classification, cancer, and hydronephrosis [4], [7] - [21]. These methods are briefly discussed here to identify pertinent issues related to the development of a new computational scheme. CKD classification is applied to analyze kidney images using statistical moment descriptors and t-tests [4]. Elongated quinary patterns and the support vector machine-radial basis function (SVM-RBF) are used to determine the presence or absence of CKD in US images [7]. Gray-level co-occurrence matrix (GLCM) features were processed with the SVM classifier to identify CKD stage in [8]. In another method, the kidney cortex area was estimated to distinguish between normal tissue and CKD stages [9]. Serum creatinine level was mapped with the cortex to identify CKD stages [10]. Recently, we proposed a scheme to identify CKD stages using 14 GLCM features and a linear discriminant analysis classifier [11]. GLCM features and an artificial neural network classifier were used to identify CKD as normal, mild, or severe in [12]. In another scheme, GFR values were mapped with US kidney images and ResNet as a classifier was used to predict kidney functions [13]. Kidney cysts are round fluid-filled sacs that form within the kidney or on the kidney. Active contour and level-set methods were used for the segmentation of single and multiple cysts [14]. The whale optimization algorithm was used to categorize kidney cysts and tumors [15]. A computing method based on K-nearest neighbor was used to classify normal kidneys, kidneys with one cyst, and kidneys with multiple cysts [16]. In another work, a multiresolution-based decomposition method was used to detect cysts in US kidney images [17]. A computing method based on a residual learning network to detect kidney abnormalities among cysts, tumors, stones, and the normal state was proposed in [18]. A metaheuristic SVM classifier for the detection of renal calculi or kidney stones was

proposed in [19]. Morphological segmentation and an ensemble multiple-support vector machine were used to identify kidney stones and cysts in [20]. A CNN-based computing scheme was proposed for the diagnosis of hydronephrosis and the normal state of the kidneys [21].

From the literature, it has been observed that there are many studies on CKD stage classification and the detection of kidney cysts, kidney stones, kidney cancer, and hydronephrosis. Detection of the amount of nephron loss in the human kidney is an important part of CKD diagnosis and treatment. Nephron loss indirectly indicates the amount of deterioration happening in a specific region of the kidney. This plays a significant role in the diagnosis and treatment of the disease relevant to the specific kidney part. Therefore, it is important to detect the amount of nephron loss during CKD progression. However, this particular aspect is missing in the literature. A computational scheme is required that could provide data on the actual or relative loss of nephrons in different kidney regions when CKD progresses with respect to a normal kidney. In this paper, we propose a computation scheme to estimate the relative amount of nephron loss in the cortex and medulla regions with respect to normal kidneys during CKD progression. A proposed pattern-matching scheme is also used to develop a computation scheme to identify CKD stages.

2. Materials and methods

This section discusses the collection and sorting of the image dataset and the methods used to identify CKD stages and amounts of nephron damage within kidney regions at different CKD stages.

2.1. Image dataset

As there is no standard dataset available in the literature to study CKD, we prepared the required dataset for this study with the help of two experienced radiologists of a radiology center (Shivam Diagnostics, Jalgaon, Maharashtra, India). We received written consent from the chief radiologist of Shivam Diagnostics to receive human adult kidney images for use in this research work related to CKD stage identification. We also received consent for consultation with their doctors and to obtain necessary advice related to the research work. Kidney images free of scars, stones, cysts, tumors, hydronephrosis, or any other ailments were included in this work. CKD stage labeling and the sorting of images was done with the help of a radiologist. US kidney images were captured using an ultrasound machine (Hitachi Aloka S-60) with a convex probe in video format, each of size 4–6 MB. Video frames of suitable views were saved in .bmp image format. All the images were preprocessed using a median filter of size 3×3 to remove speckle noise and each pixel in an image was 24 bits wide. With the help of the radiologists, each image was cropped manually to avoid a complex segmentation approach. After cropping, the file size of each US image varied between 75 and 202 KB. The region of interest was identified and unrelated information embedded within the image was removed. The human kidney has two major functioning regions: the cortex and medulla [2]. Figure 1 shows the cortex and medulla regions of a normal kidney and kidneys in different CKD stages. Figure 1 also shows US sample images of stagewise CKD progression from normal to stage-5.

In this figure, the progression of CKD from normal to stage-5 can be seen as an increase in the gray value of pixels. One can observe from Figure 1 that there is an increase in the gray value of pixels within the kidney regions with the progression of CKD stages. As per the observation of the radiologists, higher gray values of pixels represent dead nephrons. Figure 1 shows a normal US kidney image with a large number of pixels possessing lower gray values. Pixels with lower gray values represent more functioning nephrons. As CKD progresses towards higher stages, pixel gray values also increase, which represents a large amount of nephron

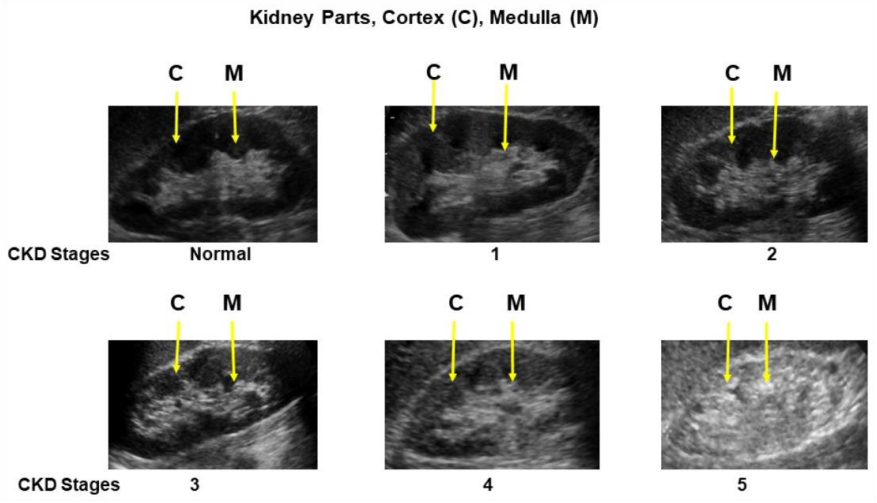

Figure 1. Stagewise CKD progression and effect of CKD progression in cortex and medulla of a human kidney in US images.

damage. In the US image of stage-5, a majority of the nephrons have higher gray values, which indicates that the kidney has lost large amounts of functioning nephrons. Semiautomatic and automatic segmentation methods do not work for the extraction of cortex and medulla data due to the complex embedding patterns of these regions. Manual segmentation was used under the supervision of radiologists for identification and precise extraction of the cortex and medulla regions [22]. Manual segmentation was performed in MATLAB 2021.

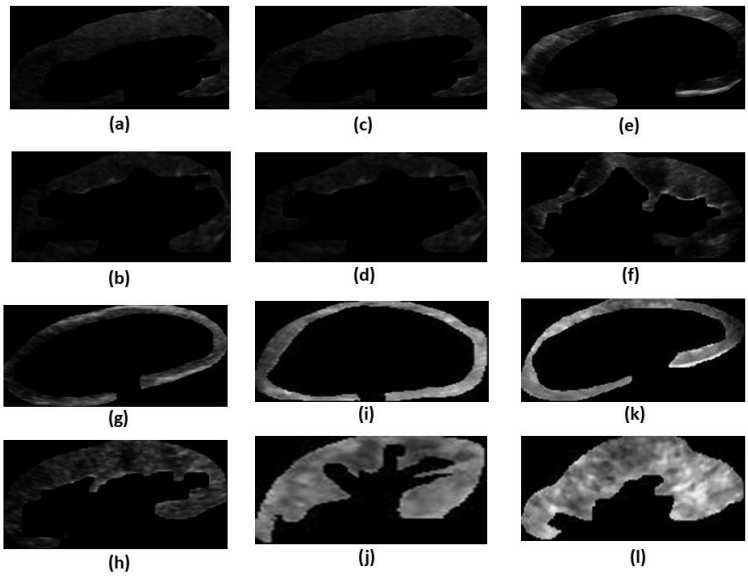

Figure 2. Segmented regions of cortex and medulla of normal kidney and different CKD stages: (a) cortex of normal kidney (CN), (b) medulla of normal kidney (MN), (c) cortex of stage-1 CKD (CS1), (d) medulla of stage-1 CKD (MS1), (e) cortex of stage-2 CKD (CS2), (f) medulla of stage-2 CKD (MS2), (g) cortex of stage-3 CKD (CS3), (h) medulla of stage-3 CKD(MS3), (i) cortex of stage-4 CKD (CS4), (j) medulla of stage-4 CKD (MS4), (k) cortex of stage-5 CKD (CS5), (l) medulla of stage-5 CKD (MS5).

The segmented regions of the cortex and medulla are shown in Figure 2. From Figure 2 one can observe that the gray values of pixels in the segmented images are gradually increasing for higher CKD stages. Similarly to Figure 1, from Figure 2 it can be observed that the segmented cortex region of the normal kidney possesses more pixels with low gray values and pixel gray values increase according to the progression of CKD stage. Therefore, the segmented regions possessing pixels with increased gray values represent larger numbers of dead nephrons in those regions.

3. Experimental setup

This section discusses the methods for estimation of damaged nephrons within the internal kidney regions and presents a template-based approach for CKD stage identification.

A computational scheme is proposed to identify the amount of nephron loss in kidney regions. Some kind of pattern matching is to be applied to US kidney images to identify nephron loss. All US kidney images of the dataset were captured at different times and with variations in the angle of the probe. This was due to variations of subjects at the radiology center. Considering these two major factors, and from the literature, for texture/pattern matching the amount of similarity is identified using standard methods such as image registration (IR) and the structural similarity index (SSIM). SSIM and IR are used to find intensity similarity and structural similarity between two images captured at different times and different angles. The cortex and medulla of a normal kidney are compared with those of different CKD stages using US images for texture/pattern matching.

About 700 US kidney images were collected at the above-mentioned radiology center in the last two years and these images are considered in this work. Not all 700 collected images reflect CKD stages. Of these 700 images, 33 images are of normal kidneys and 363 images reflect the five different CKD stages. The remaining images portray other kidney ailments such as stones, cysts, or hydronephrosis. The CKD stagewise distribution of the collected images is as follows: normal, 33 images; stage-1, 95 images; stage-2, 104 images; stage-3, 84 images; stage-4, 40 images; stage-5, 40 images. Due to the smaller numbers of collected images for normal kidneys and stage-4 and stage-5, we considered only 30 images of each CKD stage including the normal state for this work to avoid any bias of particular CKD stages while averaging the results. Out of these 700 kidney images, 30 images for each of the six stages (normal, stage-1, stage-2, stage-3, stage-4, and stage-5) were chosen. These images were manually segmented to extract the cortex and medulla. Therefore, 60 images with segmented regions obtained from 30 images of each CKD stage and a total of 360 segmented images of the cortex and medulla were obtained for normal kidneys and the five CKD stages. Segmented images of particular regions of the cortex/medulla were compared for similarity with segmented images of the same region of the next higher CKD stage. For this image comparison, the IR and SSIM methods were used. MATLAB 2021 software was also used for this purpose.

3.1. Image registration

Image registration (IR) aligns two images of the same scene taken at different times from different views. IR compares two images, where one is the reference image and the other is the target image [23]. It does not matter which image will be the reference from the image taken at different times, but selection of the reference image plays a vital role in finding the similarity index value. Hence, the reference image was selected by the radiologists only. The reference image must be from the class of normal kidneys, as we are finding similarity values with respect to normal kidney images. Because of variations in the sizes of normal kidneys (due to region,

race, etc.), similarity index values will vary marginally, which does not affect the overall result much. We also tested similarity index values by selecting different images of normal kidneys and found that using different images of normal kidneys does not affect the result much. Care must be taken while selecting reference images of normal kidneys. Hence, in this regard, the role of the radiologist is important. If the reference image is selected from any CKD stage, it will substantially affect the overall result. The intertemporal interval was set to be equal for all individuals. This helped provide uniformity in the acquisition of images.

In this research, a monomodal US image-based registration algorithm was used to find the similarity index between two images by comparing the intensity of two US images [24]. The monomodal IR method uses four types of parametric transforms: similarity, affine, rigid, and translation [23].

Similarity transform performs translation, rotation, and scaling dissimilarity between the reference image and target image. It can be expressed as follows:

$$X = xscos\theta - yssin\theta + h \tag{1}$$

$$Y = xscos\theta + yssin\theta + k \tag{2}$$

Here, s, θ, and (h, k) are scaling, rotation, and translation dissimilarity between the images. The angle between the lines is used to define the rotational dissimilarity. In an image, the ratio of distance between points is used to define the scaling difference between the images.

Affine transform preserves lines and parallelism of lines between a reference image and a target image [25]. Affine transform can do rotation, translation, and shearing of images. It can be expressed as follows:

$$[[x_i; y_i]; [X_i; Y_i]i = 1, 2, 3...] \tag{3}$$

Here, i represents the i^{th} image.

$$\begin{bmatrix} X \\ Y \\ 1 \end{bmatrix} = \begin{bmatrix} a_{11} & a_{12} & a_{13} \\ a_{21} & a_{22} & a_{23} \\ 0 & 0 & 1 \end{bmatrix} \begin{bmatrix} x \\ y \\ 1 \end{bmatrix} \tag{4}$$

a_{11}, a_{12}, a_{21}, and a_{22} specify aggregate scaling, rotation, reflection, and shearing and a_{13} and a_{23} specify the translation.

Rigid transform translates and rotates a reference image and target image to achieve correspondence between them [25]. It detects small changes in object shape, small changes in object intensity, straightness of lines, and nonzero angles between straight lines. It can be expressed as follows:

$$T_{linear}(x, y) = \begin{bmatrix} a^{'} \\ b^{'} \end{bmatrix} = R. \begin{bmatrix} a \\ b \end{bmatrix} + \begin{bmatrix} t_x \\ t_y \end{bmatrix} \tag{5}$$

Here, R is the rotation matrix and t is the translation vector.

Translation transform can do rotation and translation of target images to map them with reference images. It uses two parameters, unlike rigid transform. It can be expressed as follows:

$$f_{Translation}(x, y) = f(T_x + T_{x,y} + T_y) \tag{6}$$

$\mathbb{T}_x$ and $\mathbb{T}_y$ are horizontal and vertical translations.

All above-mentioned transforms are used for the monomodal IR method. Considering the monomodal nature of US kidney images, another image similarity measure known as the structural similarity index (SSIM)

is also used in this research. The SSIM is designed as a heuristics approach not derived from any specific image formation model [26]. It assesses the visual impact of changes in image luminance, contrast, and structure. All these parameters are separable [26].

3.2. Structural similarity index algorithm

Pixels of an image demonstrate strong dependencies and these dependencies carry useful information about the structure of a scene. SSIM exploits the pixel dependencies to model the structural information of an image [26]. It measures image similarity by assessing the visual impact of changes in three components, luminance (l), contrast (c), and structure (s), between two images x and y. These are defined as follows:

$$l(x,y) = \frac{2\mu_x\mu_y + C_1}{\mu_x^2 + \mu_y^2 + C_1} \tag{7}$$

$$c(x,y) = \frac{2\sigma_x\sigma_y + C_2}{\sigma_x^2 + \sigma_y^2 + C_2} \tag{8}$$

$$s(x,y) = \frac{\sigma_{xy} + C_3}{\sigma_x\sigma_y + C_3} \tag{9}$$

Here, μ_x and μ_y are the mean intensity of the pair of images under comparison, defined as follows:

$$\mu_x = \frac{1}{NM}\sum_{i=1}^{N}\sum_{j=1}^{M} x(i,j) \tag{10}$$

$$\mu_y = \frac{1}{NM}\sum_{i=1}^{N}\sum_{j=1}^{M} y(i,j) \tag{11}$$

N and M are the width and height of an image, and $x(i,j)$ represents the i^{th} row and j^{th} column of image x. σ_x and σ_y are the standard deviations of image x and y, defined as follows:

$$\sigma_y = (\frac{1}{NM-1}\sum_{i=1}^{N}\sum_{j=1}^{M} y(i,j) - \mu_y)^{1/2} \tag{12}$$

$$\sigma_y = (\frac{1}{NM-1}\sum_{i=1}^{N}\sum_{j=1}^{M} y(i,j) - \mu_y)^{1/2} \tag{13}$$

σ_{xy} is the sample correlation between coefficients x and y. C_1, C_2, and C_3 [26] are constant numbers greater than zero to stabilize the computation of Eqs. (7), (8), and (9) and prevent the denominators of Eqs. (7), (8), and (9) from becoming zero to avoid unstable results [26]. The overall similarity measure between images x and y is estimated using the following relation:

$$SSIM(x,y) = [l(x,y)]^{\alpha}[c(x,y)]^{\beta}[s(x,y)]^{\gamma} \tag{14}$$

Here, parameters α, β, and γ for $\alpha > 0$, $\beta > 0$, and $\gamma > 0$ mediate the relative importance of the three components.

4. Results and discussion

For estimation of nephron loss, IR with different transforms and the SSIM index algorithm help to identify the similarity between two images. The comparison of an image from one stage with images of the next stage gives a similarity value. A high similarity value (towards 1) signifies that images are more identical to each other. In other words, high similarity values represent a smaller amount of nephron loss.

4.1. Estimation of nephron loss within internal kidney regions at different CKD stages

As discussed earlier, out of 700 collected kidney images, 30 images were chosen for each of the six stages (normal, stage-1, stage-2, stage-3, stage-4, and stage-5). Therefore, 30 manually segmented images of the cortex and medulla were obtained from each set of 30 images of a particular CKD stage, and a total of 360 segmented images of the cortex and medulla were obtained from normal kidneys and five CKD stages. All images of the cortex were scaled at 651×1366 and all images of the medulla were scaled at 235×450 pixel size. Images were rescaled to this size because this was the smallest dimension of one image in the dataset.

One segmented image of a normal kidney was randomly chosen with the help of radiologists and labeled as a reference image, which was compared to 30 segmented images of the same kidney region for a particular CKD stage labeled as target images. For example, one image of the cortex of a normal kidney was compared with a set of 30 segmented images of cortexes of stage-1. Similarly, the same reference image of the cortex of a normal kidney was compared with another set of 30 images of cortexes of stage-2, and so on. In a similar manner, segmented images of the medulla of a normal kidney were compared with segmented images of the medulla of different CKD stages to estimate the similarity values. Comparison of the reference and target image pairs was performed using different image registration transforms.

The average similarity values of 30 pairs of segmented images of two different CKD stages were estimated using different IR transforms. The estimated values are listed in Table 1. Similarity values were normalized to 1. A similarity value of 1 is considered to be 100%, which indicates that there is no damage to the nephrons of the target image when compared to the reference image. Table 1 represents the average similarity values between different regions of normal kidneys and different CKD stages using different IR transforms.

Table 1. Average similarity values between different regions of normal kidneys and CKD stages. S1 - CKD stage-1, S2 - CKD stage-2, S3 - CKD stage-3, S4 - CKD stage-4, S5 - CKD stage-5.

CKD stages	Image registration transforms				Kidney region
	Similarity	Affine	Rigid	Translation	
Normal-S1	0.70	0.69	0.67	**0.66**	Cortex
Normal-S2	0.71	0.71	0.70	**0.70**	
Normal-S3	0.71	0.70	0.69	**0.69**	
Normal-S4	0.70	0.69	0.65	**0.65**	
Normal-S5	0.69	0.68	0.64	**0.64**	
Normal-S1	0.57	0.57	0.57	**0.54**	Medulla
Normal-S2	0.57	0.58	0.57	**0.54**	
Normal-S3	0.52	0.51	0.50	**0.48**	
Normal-S4	0.50	0.49	0.47	**0.44**	
Normal-S5	0.49	0.48	0.44	**0.42**	

Table 1 lists the estimates of the relative loss of nephrons in the cortex and medulla regions of different CKD stages with respect to normal kidneys. From Table 1, it is observed that the average similarity values between normal kidneys and different CKD stages of the cortex region are approximately 70%, 69%, 67%, and

67% using similarity, affine, rigid, and translation transforms, respectively. The similarity values between normal kidneys and different CKD stages of the medulla region are about 53%, 53%, 51%, and 49% using similarity, affine, rigid, and translation transforms, respectively. For each transform and for all stages, the vertical average is considered. Furthermore, Table 1 shows that the IR method with translation transform estimates relative nephron loss in the cortex region of stage-1 to stage-5 with regard to normal kidneys varying between 34% and 36%. Similarly, the relative nephron loss in the medulla region of stage-1 to stage-5 with regard to normal kidneys varies between 46% and 58%. Therefore, the estimates of nephron loss shown in Table 1 vary widely between CKD stages and kidney regions.

As shown in Table 1, IR with translation transform outperforms the other transforms because of its properties such as overlapping the anatomical objects in both images as much as possible by resolving the translational misalignment between the images by preserving the size of the image object [27]. In the cortex and medulla regions, IR with translation transform captures the progressive loss of nephrons as CKD stages progress and it outperforms the other transforms. In the cortex for stage-1 to stage-5, the similarity value is almost 66%, which indicates almost 34% nephron damage due to CKD progression. In the medulla for stage-1 to stage-5, the similarity value is almost 49%, which indicates almost 51% nephron damage due to CKD progression. As shown in Table 1, nephron loss varies from almost 34% up to 51% in different regions of the kidney. Therefore, the nephron losses estimated by the proposed scheme are very much in conformity with the observations of radiologists based on clinical data. The SSIM index values of the cortex and medulla from US images of different pairs of CKD stages were also estimated. The estimated values are listed in Table 2.

Table 2. Average similarity values using SSIM index algorithm between normal kidneys and different CKD stages. S1 - CKD stage-1, S2 - CKD stage-2, S3 - CKD stage-3, S4 - CKD stage-4, S5 - CKD stage-5.

SSIM index algorithm			
Cortex		**Medulla**	
Normal-S1	0.62	Normal-S1	0.50
Normal-S2	0.67	Normal-S2	0.46
Normal-S3	0.67	Normal-S3	0.44
Normal-S4	0.64	Normal-S4	0.42
Normal-S5	0.64	Normal-S5	0.40

From Table 2, it is observed that the average similarity values between the cortex region of normal kidneys and different CKD stages is almost 65%, which indicates that there is almost 35% nephron damage in the cortex region of different CKD stages compared to normal kidneys. Similarly, the average similarity values between the medulla region of normal kidneys and different CKD stages is found to be 44%, which indicates that there is almost 56% nephron damage in the medulla region of different CKD stages compared to normal kidneys. For all stages, the vertical average is considered. It is also observed from Table 2 that, at different CKD stages (from normal to stage-1 and stage-1 to stage-5), the nephron damage for the cortex region varies in the range of 33% to 38%, and for the medulla region it varies in the range of 50% to 60%. More nephron damage occurs in the medulla region because of its large volume [28]. For identification of nephron loss, similarity values of CKD images belonging to normal kidneys are close to unity and those of stage-1 and stage-2 are marginally less than the similarity values of normal kidneys as the nephron loss is relatively less in these CKD stages. However, the similarity values of stage-3, stage-4, and stage-5 are expected to be substantially lower compared to the similarity values of normal kidneys due to high amounts of nephron loss. As shown in Table 2, the similarity values of images of CKD stages progress from normal to stage 5 with a gradual decrease as per expectations, as

the amount of nephron loss increases with the progress of CKD stages. The results shown in Table 2 are very much in conformity with the observations of the radiologists based on clinical data.

To find reasons for nephron loss, medical practitioners use autopsy procedures. With this approach, kidney sample tissues are analyzed through histopathological evaluations to identify the causes of the prevalence of the disease. Autopsy is performed after the death of the patient and has limitations like delays in carrying out the autopsy, improper sampling, and nonavailability of representative samples, which influence the correctness of the results [29].

Nephron loss can also be detected using biopsy procedures. Renal biopsy, when performed for CKD patients, may have higher risks of bleeding and does not provide in-depth information about damage. The accuracy of the results of renal biopsy are low when the kidneys are small in size, particularly in CKD stage-3 to stage-5. The proposed method is noninvasive and detects the amount of nephron loss of living humans of any age, without performing any extra tests like eGFR or biopsy. The amount of damage identified by the IR algorithm and SSIM algorithm reflects the overall damage of nephrons in the kidney cortex and medulla regions. From Table 1 and Table 2, it is observed that a gradual decrease in functioning nephrons takes place in different kidney regions due to CKD progression. Early identification of nephron damage in kidney regions will assist nephrologists in drawing first-hand conclusions and deciding on a course of treatment.

4.2. CKD stage identification using similarity index

This section discusses a novel template-based approach for CKD stage identification. We have shown that the nephron damage in different kidney regions during CKD progression can be estimated using similarity index values. While computing similarity values for the estimation of nephron loss, we found that the IR and SSIM methods can also be used for CKD stage identification. There is a twofold advantage when the similarity index is used for CKD stage identification, as only one method will be used for the identification of CKD stage and nephron damage in kidney regions and the similarity index method does not require multiclass classifier and parameter settings for the classification of CKD stages. Keeping this in mind, in this paper, we propose a computing method based on the similarity index for CKD stage identification. The proposed method classifies CKD stages in two steps. In step-1, similarity index threshold values are determined for different CKD stages, and then the threshold values are used to classify the CKD stage in step-2. Figure 3 shows a stepwise flow diagram for CKD stage identification using IR and the SSIM algorithm.

Initially, US kidney images belonging to CKD stages were collected and sorted. Normal kidney images and CKD images were segregated into a training set and test set. In the training phase, a reference image was selected and compared to images of normal kidneys and CKD stage-1, stage-2, stage-3, stage-4, and stage-5. Minimum and maximum similarity index values were identified to create a table of stagewise threshold values and approximation was done. In the testing phase, comparisons of images were done and the obtained similarity values were mapped with stagewise defined threshold values for identification of CKD stages. A template-based approach for CKD stage identification is discussed in the following section.

4.2.1. Determination of threshold values of CKD stages

As discussed in Section 3, out of the collected 700 US images of normal kidneys and five CKD stages, 396 images were found suitable and were considered for step-1 and step-2 of the proposed method. The selected 396 images were split in a ratio of 80:20 for use in step-1 and step-2 of the proposed scheme. Therefore, 330 images (normal: 22 images, stage-1: 84 images, stage-2: 93 images, stage-3: 73 images, stage-4: 29 images, and stage-5:

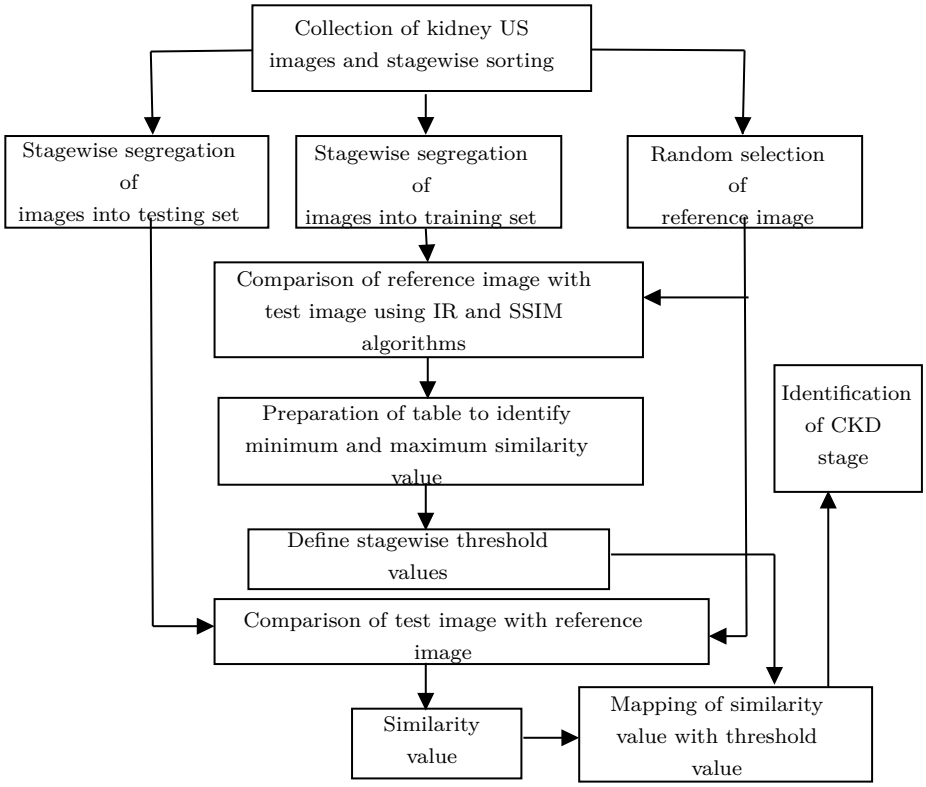

Figure 3. Flow diagram for CKD stage identification using IR and SSIM algorithm.

29 images) were used in step-1 of the proposed scheme to determine the threshold values of the similarity index while the remaining 66 images of the total selected images were used in step-2 to identify the CKD stage. From the selected images, 66 images, i.e., 11 images each for normal kidneys and the five CKD stages, were segregated for step-2. All selected US kidney images were manually segmented before they were used in step-1 and step-2. After manual segmentation, all kidney images were rescaled at dimensions of 196×293. Images were rescaled to this size because this was the smallest dimension of one of the images in the dataset. Figure 4 shows manually segmented images of normal kidneys and the five CKD stages.

From Figure 4, one can observe that whole kidney images are considered in step-1 and step-2. To avoid complexity of the segmentation process, these whole kidney images are manually segmented under the supervision of radiologists to have a precise kidney structure [22]. For determination of similarity index values, one US image of a normal kidney (labeled as the reference image) is chosen randomly with the help of radiologists from the available dataset. The reference image is compared with the remaining normal kidney images, as kidney size differs from person to person of different regions [2]. The same reference image is compared with images of stage-1 through stage-5 in step-1. Image comparisons are done using the IR algorithm with similarity transform and the SSIM index algorithm. From image comparison results, minimum and maximum similarity index values of each CKD stage are estimated using the IR algorithm with similarity transform as shown in Table 3.

As shown in Table 3, the actual minimum and actual maximum similarity values of two adjacent stages are not continuous. There is a clear gap between them. If the actual minimum and maximum similarity values of each CKD stage are considered as the threshold values, then in step-2, the similarity index of the test image may fall in the gap of the threshold values, and that creates ambiguity in predicting the CKD stage of the test image.

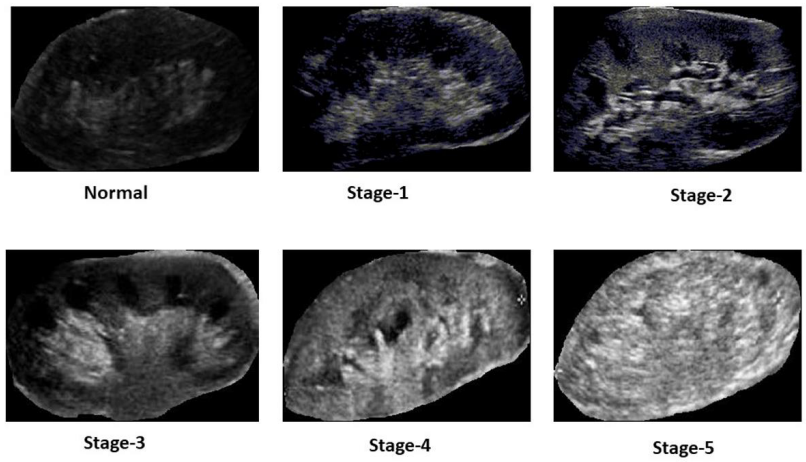

Figure 4. Segmented US images of different CKD stages.

Table 3. Estimated threshold values of image comparisons using IR algorithm with similarity transform, where δM_i and ΔM_a are $\Delta M_i/2$, $\Delta M_a/2$. Legend: Mi: actual minimum value, Ma: actual maximum value, AMi: approximate minimum value, AM_a: approximate maximum value, Avg.: average.
Avg= $(M_i+M_a)/2$, $\Delta M_i = M_i$ – Avg., ΔMa = Ma – Avg., $AM_i = M_i + \delta M_i$, $AM_a = M_a + \delta M_a$

Stage	Actual value		Avg.	Difference (Δ)		δMi	δMa	Approximate		Rounded off	
	Min. (Mi)	Min. (Ma)		ΔMi	δMa			AMi	AMa	[AMi]	[AMa]
N	0.92	0.99	0.96	-0.03	+ 0.03	-0.02	+0.02	0.91	1.01	0.91	1.0
1	0.87	0.90	0.88	-0.02	+ 0.02	–0.01	+0.01	0.86	0.90	0.86	0.90
2	0.595	0.79	0.69	-0.10	+ 0.10	–0.05	+0.05	0.54	0.85	0.54	0.85
3	0.29	0.49	0.39	-0.10	+ 0.09	–0.05	+0.05	0.24	0.53	0.24	0.53
4	0.20	0.22	0.21	-0.01	+ 0.01	–0.01	+0.01	0.19	0.23	0.20	0.23
5	0.09	0.17	0.13	-0.04	+ 0.04	–0.02	+0.02	0.07	0.19	0.07	0.19

To remove such ambiguity, actual minimum and actual maximum similarity values are approximated such that there is continuity between the lower and upper threshold values of two adjacent stages. Approximation of actual minimum and actual maximum values can be done many ways. However, we have estimated correction values (∂_{M_i}, ∂_{M_a}) to approximate actual minimum and actual maximum values. Finally, the approximate values are rounded to obtain the desired threshold values of each CKD stage. Table 3 shows calculated rounded-off approximate values, which are used as threshold values in step-2 of the computations. Similarly, we determined similarity index threshold values of CKD stages using the SSIM index algorithm and these values are given in Table 4.

4.2.2. Prediction of CKD stages using threshold values

In step-2 of the proposed scheme, 66 images of normal kidneys and the five different CKD stages are considered as test images. During step-2, test images are selected randomly from the image set of 66 images one by one and compared with reference images for calculations of similarity index values. Similar to step-1, one image is selected randomly from the images of normal kidneys as a reference image for step-2. Table 5 lists the actual CKD stage of 66 test images and the predicted CKD stage of test images obtained using the threshold values of Table 3 (IR algorithm with similarity transform).

Table 4. Estimated threshold values of image comparisons using SSIM index algorithm, where δM_i and ΔM_a are $\Delta M_i/2$, $\Delta M_a/2$. Legend: Mi: actual minimum value, Ma: actual maximum value, AMi: approximate minimum value, AM_a: approximate maximum value, Avg.: average.
Avg= $(M_i+M_a)/2$, $\Delta M_i = M_i$ – Avg., ΔMa = Ma – Avg., $AM_i = M_i + \delta M_i$, $AM_a = M_a + \delta M_a$

Stage	Actual value		Avg.	Difference (Δ)		δMi	δMa	Approximate		Rounded off	
	Min. (Mi)	Min. (Ma)		ΔMi	δMa			AMi	AMa	[AMi]	[AMa]
N	0.91	0.99	0.95	-0.04	+ 0.04	-0.02	+ 0.02	0.89	1.02	0.89	1.0
1	0.85	0.87	0.86	-0.01	+ 0.01	-0.07	+ 0.01	0.84	0.88	0.84	0.88
2	0.58	0.78	0.68	-0.09	+ 0.10	-0.05	+ 0.05	0.53	0.83	0.53	0.83
3	0.26	0.47	0.37	-0.01	+ 0.10	-0.05	+ 0.05	0.21	0.52	0.21	0.52
4	0.14	0.19	0.17	-0.02	+ 0.02	-0.01	+ 0.01	0.13	0.19	0.13	0.20
5	0.07	0.11	0.09	-0.02	+ 0.02	-0.01	+ 0.01	0.06	0.12	0.06	0.12

Table 5. Prediction of CKD stages using threshold values obtained with IR algorithm with similarity transform, where TI is test image, LI is labeled image, PS is predicted stage, and SV is similarity value.

TI	LI	SV	PS	TI	LI	SV	PS	TI	LI	SV	PS	TI	LI	SV	PS
1	S-4	0.22	S-4	17	S-2	0.69	S-2	33	S-3	0.48	S-3	50	S-2	0.66	S-2
2	S-1	0.84	S-2	18	N	0.92	N	34	N	0.91	N	51	S-5	0.12	S-5
3	S-3	0.27	S-3	19	S-1	0.90	S-1	35	S-2	0.66	S-2	52	S-3	0.39	S-3
4	S-5	0.17	S-5	20	S-5	0.05	S-5	36	S-3	0.42	S-3	53	N	0.93	N
5	S-2	0.70	S-2	21	N	0.93	N	37	S-5	0.06	S-5	54	S-2	0.86	S-1
6	S-3	0.32	S-3	22	S-4	0.25	S-3	38	S-4	0.21	S-4	55	S-1	0.88	S-1
7	S-4	0.20	S-4	23	N	0.95	N	39	S-3	0.50	S-3	56	S-2	0.72	S-2
8	S-1	0.89	S-1	24	S-1	0.86	S-1	40	S-1	0.88	S-1	57	S-3	0.38	S-3
9	S-4	0.23	S-4	25	S-2	0.69	S-2	41	S-5	0.21	S-4	58	S-5	0.11	S-5
10	S-2	0.52	S-3	26	S-3	0.44	S-3	42	N	0.97	N	59	S-4	0.23	S-4
11	N	0.91	N	27	S-4	0.15	S-5	43	S-3	0.52	S-3	60	N	0.95	N
12	S-1	0.87	S-1	28	N	0.98	N	44	S-5	0.07	S-5	61	S-1	0.86	S-1
13	S-5	0.10	S-5	29	S-2	0.66	S-2	45	N	0.94	N	62	S-4	0.22	S-4
14	S-4	0.21	S-4	30	S-1	0.86	S-1	46	S-2	0.86	S-1	63	S-3	0.30	S-3
15	S-5	0.13	S-5	31	S-4	0.21	S-4	47	S-1	0.87	S-1	64	S-2	0.74	S-2
16	S-3	0.43	S-3	32	S-5	0.16	S-5	48	S-4	0.21	S-4	65	S-1	0.92	N
								49	S-5	0.05	S-5	66	N	0.98	N

N: Normal, S-1: stage-1, S-2: stage-2, S-3: stage-3, S-4: stage-4, S-5: stage-5

Similarly, Table 6 lists the predicted CKD stages of the same set of 66 test images using the threshold values from the SSIM index algorithm of Table 4.

A confusion matrix is obtained using the actual and predicted CKD stages of the 66 test images of Table 5 and Table 6. The confusion matrix is used to estimate the accuracy of the proposed scheme in predicting different CKD stages. It is desirable to have a confusion matrix with more diagonal elements, which represents correct identification. The off-diagonal elements of the confusion matrix represent the incorrect identification of test images [11]. Algorithm performance is considered poor when a higher number of test images fall off the diagonal in the confusion matrix. Stagewise values of the confusion matrix of Table 5 and Table 6 are shown in Figure 5. These parameter values are used to estimate prediction accuracy of individual CKD stages and the overall accuracy rates of all six stages are estimated using the formulas of Eqs. (15) and (16). The i^{th} stagewise

Table 6. Prediction of CKD stages using threshold values obtained with the SSIM index algorithm, where TI is test image, LI is labeled image, PS is predicted stage, and SV is similarity value.

TI	LI	SV	PS	TI	LI	SV	PS	TI	LI	SV	PS	TI	LI	SV	PS
1	S-4	0.28	S-3	17	S-4	0.18	S-5	33	N	0.93	N	50	S-2	0.88	S-1
2	S-1	0.69	S-2	18	S-1	0.86	S-1	34	S-2	0.78	S-2	51	S-1	0.84	S-2
3	S-2	0.51	S-3	19	S-3	0.44	S-3	35	S-5	0.11	S-5	52	S-3	0.43	S-3
4	S-1	0.86	S-1	20	S-4	0.22	S-4	36	N	0.94	N	53	S-4	0.21	S-4
5	N	0.92	N	21	S-2	0.86	S-1	37	S-1	0.92	N	54	S-5	0.08	S-5
6	S-2	0.79	S-2	22	S-3	0.22	S-4	38	S-3	0.21	S-4	55	S-1	0.89	S-1
7	S-4	0.21	S-4	23	S-5	0.20	S-4	39	S-4	0.22	S-4	56	S-2	0.70	S-2
8	S-5	0.21	S-4	24	S-3	0.83	S-2	40	S-5	0.13	S-5	57	S-3	0.81	S-2
9	N	0.93	N	25	S-2	0.49	S-3	41	S-4	0.17	S-5	58	N	0.97	N
10	S-4	0.20	S-4	26	S-1	0.73	S-2	42	N	0.94	N	59	S-3	0.49	S-3
11	S-5	0.12	S-5	27	S-4	0.21	S-4	43	S-1	0.88	S-1	60	S-5	0.14	S-5
12	S-5	0.09	S-5	28	S-3	0.39	S-3	44	S-3	0.46	S-3	61	S-5	0.14	S-5
13	S-3	0.84	S-2	29	N	0.96	N	45	N	0.90	N	62	S-5	0.13	S-5
14	S-1	0.81	S-2	30	S-1	0.87	S-1	46	S-2	0.80	S-2	63	S-4	0.20	S-4
15	N	0.92	N	31	S-2	0.48	S-3	47	S-4	0.14	S-5	64	S-2	0.86	S-1
16	S-2	0.74	S-2	32	S-5	0.14	S-5	48	N	0.92	N	65	S-3	0.79	S-2
								49	N	0.91	S-1	66	S-1	0.87	S-1

N: Normal, S-1: stage-1, S-2: stage-2, S-3: stage-3, S-4: stage-4, S-5: stage-5

Stage		Actual					
		Normal	1	2	3	4	5
Predicted	Normal	11	1				
	1		9	2			
	2		1	8			
	3			1	11	1	
	4					9	1
	5					1	10

(a) Confusion matrix of Table 5 for IR with similarity transform

Stage		Actual					
		Normal	1	2	3	4	5
Predicted	Normal	10	1				
	1	1	6	3			
	2		4	5	4		
	3			3	5	1	
	4				2	7	2
	5					3	9

(b) Confusion matrix of Table 6 for SSIM index algorithm

Figure 5. Confusion matrix.

accuracy (Ai) can be computed using the following formula:

$$A_i = \frac{TP_i + TN_i}{TP_i + TN_i + FP_i + FN_i} \tag{15}$$

Here, TPi represents the correct classification of the i^{th} stage's test image. FPi represents the incorrect classification of the i^{th} stage's test images into other stages. FNi represents the incorrect classification of other stage's test images into the i^{th} stage. TNi represents the number of test images not influencing the identification of the i^{th} stage.

From Figure 5, one can observe that the confusion matrix of Table 5 for IR with similarity transform has more diagonal elements, which shows that IR with similarity transform identifies CKD stages with better accuracy.

On the other hand, the confusion matrix of Table 6 for the SSIM index algorithm has comparatively fewer diagonal elements, which represents poor classification results.

Aggregate accuracy (AA) can be computed using the following formula:

$$AA = \frac{\sum_{i=1}^{S} A_i}{S} \tag{16}$$

Here, A_i represents the stagewise classification accuracy of the i^{th} stage and S represents the total number of stages. Stagewise prediction accuracy and aggregate accuracy of IR (with similarity transform) and the SSIM index algorithm are estimated using Eqs. (15) and (16).

We also estimated the stagewise and aggregate prediction accuracy of the same set of test images using the GLCM-based method of [11] and the SVM-based method of [30] for comparison. The estimated values are listed in Table 7.

Table 7. Comparison of prediction accuracy of image registration (with similarity transform) and SSIM index algorithm methods.

Algorithms	**Stagewise**						**Aggregate**
	Normal	Stage-1	Stage-2	Stage-3	Stage-4	Stage-5	
IR with similarity transform	**98.48**	**93.93**	**93.93**	**96.96**	**95.45**	**96.96**	**95.95**
SSIM index	96.96	86.36	78.78	84.84	87.87	92.42	87.87
GLCM-based method [11]	96	96	100	98	96	95	96.83
SVM-based method [30]	45	26	69	76	90	90	66.00

As shown in Table 7, the prediction accuracy of the IR algorithm for identifying individual CKD stages is higher than the prediction accuracy of the SSIM index algorithm. Among the existing methods, the GLCM-based image classification method of [11] has higher prediction accuracy than the prediction accuracy of the SVM-based method of [30]. Compared with the GLCM-based classification method of [11], the prediction accuracy of the proposed method based on IR with similarity transform provides the same or better prediction accuracy for three CKD stages (normal, stage-4, and stage-5), while the prediction accuracy rates of two CKD stages (stage-1 and stage-3) are marginally lower (within 2%) than those of [11]. The aggregate prediction accuracy of the proposed method based on the IR algorithm with similarity transform is almost identical to that of [11]. Overall, the prediction accuracy offered by the IR algorithm has performance comparable to that of the GLCM-based image classification method for identifying CKD stages. The IR algorithm with similarity transform provides better results for identifying CKD stages. This is because of properties of similarity transform such as preserving shape and angles between lines but not size [27]. The proposed method is simple and straightforward compared to the existing image classification methods of [11] and [30]. Therefore, the proposed computing method based on pattern matching is a better alternative to existing image classification-based methods for CKD stage identification.

5. Conclusion

In this paper, a novel pattern matching-based computation scheme has been proposed to detect nephron loss in different kidney regions due to CKD progression. We have considered the IR algorithm with different transforms and the SSIM algorithm for pattern matching of different kidney regions to identify nephron loss. Simulation results showed that the proposed scheme based on the IR and SSIM algorithms detects almost 34% and 51% and almost 35% and 56% nephron damage in the cortex and medulla relative to normal kidneys, respectively,

due to CKD progression. It was also observed from the results that the IR algorithm with translation transform offered better results compared to the other IR transforms for detection of nephron loss in the cortex and medulla of the kidneys. When the performance of the IR algorithm was compared to the SSIM algorithm, we observed that the IR algorithm with translational transform was able to detect nearly 2% to 4% higher nephron loss relative to normal kidneys than the SSIM. Therefore, the IR algorithm with translational transform is the better choice over the SSIM to estimate relative nephron loss due to CKD progression. The limitation of this study is that it did not identify the absolute amount of damaged nephrons. We have also proposed a computing scheme to identify CKD stages using a novel pattern matching method. The proposed method does not use a classifier, unlike the existing schemes. Instead, it uses a reference table of threshold values obtained during the training phase for stage classification. Furthermore, simulation results showed that the proposed scheme based on IR with similarity transform and the SSIM algorithm can identify CKD stages with accuracy of 96% and 88%, respectively. The prediction accuracy of the proposed scheme for identifying CKD stages using IR with similarity transform is comparable to that of the GLCM-based image classification method, which is the best among the existing methods. The proposed scheme has a few advantages over the existing computing scheme for CKD stage identifications, such as: (i) the proposed method is simple and straightforward; (ii) it can be used to identify both CKD stages and nephron loss during CKD progression; (iii) there is no need for feature extraction and selection of contributing features; and (iv) it does not require the classification stage, unlike the existing schemes. Overall, the proposed IR-based computing method can be used for CKD stage identification and to estimate relative nephron loss with respect to normal kidneys. Therefore, the proposed computation scheme is a better alternative to the existing schemes proposed for CKD stage identification. The proposed scheme does not provide the exact estimate of the nephron loss in the kidney regions and that is its only limitation.

Acknowledgment

The authors gratefully acknowledge Dr. Kiran Patil (MD, radiologist) at Shivam Diagnostics Jalgaon, Maharashtra, India, for clearance of legal and ethical procedures, collection of US kidney images, identification of CKD stages, and long hours of discussion of medical terms. We also thank Dr. Aleem Ansari, Medical Officer at District Civil Hospital, Dhule, Maharashtra, India, for guidance on CKD stages and nephron functions. We extend our heartfelt gratitude to Dr. Amit Page, Assistant Professor, School of Pharmacy and Technology Management, SVKM's NMIMS Shirpur Campus, for helping with the literature on nephrons and enlightening us about minute structural and functional details of the nephrons and kidneys.

R.A. worked on conceptualization, methodology, data collection, investigation, experimentation, and manuscript preparation. B.K.M. worked on methodology, visualization, draft editing, and review.

References

[1] Hadi F, Anita L, Vallon V. How do kidneys adapt to a deficit or loss in nephron number? Physiology 2019; 34: 189-197. http://dx.doi.org/10.1152/physiol.00052.2018

[2] Bertram JF, Boucar R, Diouf N, Hughson MD, Hoy WE. Human nephron number: implications for health and disease. Pediatric Nephrology 2011: 26; 1529-1533. http://dx.doi.org/10.1007/s00467-011-1843-8

[3] Feher J. Quantitative Human Physiology: An Introduction. Chennai, India: Academic Press-Elsevier, 2012.

[4] Ardiatna W, Saputro A, Soejoko D. Analysis of kidney ultrasound images characterization using statistical moment descriptor. In: 2018 International Conference on Computer, Control, Informatics and Its Applications; Tangerang, Indonesia; 2018. pp. 17-22.

[5] Dhaun N, Bellamy C, Cattran D, Kluth D. Utility of renal biopsy in the clinical management of renal disease. Kidney International 2014; 85: 1039-1048. http://dx.doi.org/ 10.1038/ki.2013.512

[6] Hsieh J, Lee C, Chen Y, Lee W, Chiang H. Stage classification in chronic kidney disease by ultrasound image. In: Proceedings of the 29th International Conference on Image and Vision Computing; Hamilton, New Zealand; 2014. pp. 19-21.

[7] Acharya U, Meiburger K, Koh J, Hagiwara Y, Oh S et al. Automated detection of chronic kidney disease using higher-order features and elongated quinary patterns from B-mode ultrasound images. Neural Computing and Applications 2020; 32: 11163-11172. https://doi.org/10.1007/s00521-019-04025-y

[8] Sharma K, Virmani J. A decision support system for classification of normal and medical renal disease using ultrasound images: a decision support system for medical renal diseases. International Journal of Ambient Computing and Intelligence 2017: 2 (8): 52-69. http://dx.doi.org/10.4018/IJACI.2017040104

[9] Iqbal F, Pallewatte A, Wansapura J. Texture analysis of ultrasound images of chronic kidney disease. In: 2017 Seventeenth International Conference on Advances in ICT for Emerging Regions; Colombo, Sri Lanka; 2017. pp. 1-5.

[10] Ahmed S, Bughio S, Hassan M, Lal S, Ali M. Role of ultrasound in the diagnosis of chronic kidney disease and its correlation with serum creatinine level. Cureus 2019; 11 (3): e4241. https://doi.org/10.7759/cureus.4241

[11] Ahmad R, Mohanty B. Chronic kidney disease stage identification using texture analysis of ultrasound images. Biomedical Signal Processing and Control 2021; 69: 102695. https://doi.org/10.1016/j.bspc.2021.102695

[12] Kim D, Ye S. Classification of chronic kidney disease in sonography using the GLCM and artificial neural network. Diagnostics 2021; 11: 864. https://doi.org/10.3390/diagnostics11050864

[13] Kuo C, Chang C, Liu K, Lin W, Chiang H et al. Automation of the kidney function prediction and classification through ultrasound-based kidney imaging using deep learning. NPJ Digital Medicine 2019; 2: 29. https://doi.org/10.1038/s41746-019-0104-2

[14] Akkasaligar PT, Biradar S. Automatic kidney cysts segmentation in digital ultrasound images. In: Shukla A (editor). Medical Imaging Methods. Prayagraj, India: Springer Nature Singapore, 2019. pp. 97-117. https://doi.org/10.1007/978-981-13-9121-7_4

[15] Raju P, Rao VM, Rao BP. Optimal GLCM combined FCM segmentation algorithm for detection of kidney cysts and tumor. Multimedia Tools & Applications 2019; 78: 18419-18441. https://doi.org/10.1007/s11042-018-7145-4

[16] Akkasaligar PT, Biradar S. Analysis of polycystic kidney disease in medical ultrasound images. International Journal of Medical Engineering and Information 2018; 10 (1): 49-64. https://doi.org/10.1504/IJMEI.2018.090085

[17] Eslami A, Kasaei S, Jahed M. Radial multiscale cyst segmentation in ultrasound images of kidney. In: Proceedings of the Fourth IEEE International Symposium on Signal Processing and Information Technology; Rome, Italy; 2004. pp. 42-45.

[18] Sudharson S, Kokil P. Computer-aided diagnosis system for the classification of multi-class kidney abnormalities in the noisy ultrasound images. Computer Methods and Programs in Biomedicine 2021; 205: 106071. https://doi.org/10.1016/j.cmpb.2021.106071

[19] Selvarani S, Rajendran P. Detection of renal calculi in ultrasound image using meta-heuristic support vector machine. Journal of Medical Systems 2019; 43: 300. https://doi.org/10.1007/s10916-019-1407-1

[20] Sudharson S, Kokil P. Abnormality detection in the renal ultrasound images using ensemble MSVM model. In: 2019 International Conference on Wireless Communications Signal Processing and Networking; Chennai, India; 2019. pp. 378-382.

[21] Su J, Liu Y, Wang J. Ultrasound image assisted diagnosis of hydronephrosis based on CNN neural network. Journal of King Saud University 2020; 32 (6): 2682-2687. https://doi.org/10.1016/j.jksus.2020.04.005

[22] Preim B, Botha C. Visual Computing for Medicine, Theory, Algorithms and Applications: Image Analysis for Medical Visualization. Boston, MA, USA: Morgan Kaufmann-Elsevier, 2014.

[23] Zitova B, Flusser J. Image registration methods: a survey. Image and Vision Computing 2003; 21: 977-1000.

[24] Che C, Mathai T, Galeotti J. Ultrasound registration: a review. Methods 2017; 115: 128-143. http://dx.doi.org/10.1016/j.ymeth.2016.12.006

[25] Josien P, Pluim W, Maintz JB, Viergever MA. Mutual-information-based registration of medical images: a survey. IEEE Transactions on Medical Imaging 2003; 22 (8): 986-1004. http://dx.doi.org/10.1109/TMI.2003.815867

[26] Wang Z, Bovik A, Sheikh H, Simoncelli E. Image quality assessment: from error visibility to structural similarity. IEEE Transactions on Image Processing 2004; 13 (4): 600-612. http://dx.doi.org/10.1109/TIP.2003.819861

[27] Johnson HJ, McCormick MM, Ibanez L. The ITK Software Guide: Design and Functionality. New York, NY, USA: Kitware Publisher, 2015.

[28] Aleksandar D, Richard JG, Andrew DR. Structural and functional changes with the aging kidney. Advanced Chronic Kidney Disease 2016; 23 (1): 19-28. https://doi.org/10.1053/j.ackd.2015.08.004

[29] Pratima K, Renu G, Swapnil A, Avni B, Rajani A. Spectrum of renal lesions on autopsy: experience of a tertiary level institute based on retrospective histopathological analysis. Cureus 2021; 13 (8): e17064. https://doi.org/10.7759/cureus.17064

[30] Chen C, Pai T, Hsu H, Lee C, Chen K et al. Prediction of chronic kidney disease stages by renal ultrasound imaging. Enterprise Information Systems 2019; 14: 178-195. https://doi.org/10.1080/17517575.2019.1597386